1-1-2005

Measurement and Control of Torque Ripple-Induced Frame Torsional Vibration in a Surface Mount Permanent Magnet Machine

Jason Neely

Steven Pekarek
Missouri University of Science and Technology

Daniel S. Stutts
Missouri University of Science and Technology, stutts@mst.edu

Philip Beccue

Recommended Citation

J. Neely et al., "Measurement and Control of Torque Ripple-Induced Frame Torsional Vibration in a Surface Mount Permanent Magnet Machine," *IEEE Transactions of Power Electronics*, Institute of Electrical and Electronics Engineers (IEEE), Jan 2005.
The definitive version is available at https://doi.org/10.1109/TPEL.2004.839810

Measurement and Control of Torque Ripple-Induced Frame Torsional Vibration in a Surface Mount Permanent Magnet Machine

Philip Beccue, *Student Member, IEEE*, Jason Neely, Steve Pekarek, *Member, IEEE*, and Daniel Stutts

***Abstract*—A sensor to measure the stator torsional vibration due to torque ripple produced by a surface mount permanent magnet machine is first described. The sensor is relatively inexpensive and is straight forward to incorporate into a drive system. Experiments are performed to validate that the voltage produced by the sensor is linearly related to torque ripple amplitude. Closed-loop controllers are then described that adjust the stator current harmonics applied to the machine to achieve a commanded average torque while mitigating measured torsional vibration. Simulation and experimental results are used to demonstrate the effectiveness of the control techniques.**

***Index Terms*—Closed-loop controllers, permanent magnet machine, stator current harmonics, stator torsional vibration, torque ripple.**

NOMENCLATURE

v_{xs}	"x" phase to neutral voltage.
i_{xs}	"x" phase current.
λ_{xs}	"x" phase flux linkage.
r_s	Phase resistance.
L_{xsys}	"x" to "y" phase mutual inductance.
λ_{xsm}	Influence of the flux of the permanent magnets on stator winding "x."
P	Number of poles.
p	Differentiation with respect to time (d/dt).
T_e	Electromagnetic torque.
$\bar{T}_e$	Average value of electromagnetic torque.
T_{cog}	Cogging torque expressed as a Fourier series.
T_{eqy}	Magnitude of the yth torque harmonic amplitude, including cogging torque (even Fourier series component).
T_{edy}	Magnitude of the yth torque harmonic amplitude, including cogging torque (odd Fourier series component).
$\boldsymbol{T}_{cqy}$	Magnitude of the yth cogging torque harmonic (even Fourier series component).
$\boldsymbol{T}_{cdy}$	Magnitude of the yth cogging torque harmonic (odd Fourier series component).
$\boldsymbol{T}_{\text{eq}} \in \mathbb{R}^f$	Torque harmonic coefficients in matrix form, including cogging torque (even Fourier series component).
$\boldsymbol{T}_{ed} \in \mathbb{R}^f$	Torque harmonic coefficients in matrix form, including cogging torque (odd Fourier series component).
$\boldsymbol{T}_{cq} \in \mathbb{R}^f$	Cogging torque harmonic coefficients in matrix form (even Fourier series component).
$\boldsymbol{T}_{cd} \in \mathbb{R}^f$	Cogging torque harmonic coefficients in matrix form (odd Fourier series component).
κ_{em}	Magnitude of the mth back-emf harmonic.
κ_{iqn}	Magnitude of the nth stator current harmonic (even Fourier series component).
κ_{idn}	Magnitude of the nth stator current harmonic (odd Fourier series component).
$\boldsymbol{K}_{e1} \in \mathbb{R}^{f \times g}$	A matrix containing scaled back-emf coefficients used in precise torque control algorithm (Section V-A).
$\boldsymbol{K}_{e2} \in \mathbb{R}^g$	A vector containing scaled back-emf coefficients used in the derivation of average torque in the precise torque control algorithm (Section V-A).
$\boldsymbol{K}_{e3} \in \mathbb{R}^f$	A matrix containing scaled back-emf coefficients used to derive the expression for torque ripple harmonic coefficients in the approximate control of average torque algorithm (Section V-B).
$\boldsymbol{K}_{e4} \in \mathbb{R}^{f \times (g-1)}$	A matrix containing scaled back-emf coefficients used in the approximate control of average torque algorithm (Section V-B).
$\boldsymbol{i}_q \in \mathbb{R}^g$	Stator current harmonics coefficients in matrix form (even Fourier series component).
$\boldsymbol{i}_d \in \mathbb{R}^g$	Stator current harmonics coefficients in matrix form (odd Fourier series component).

Manuscript received October 15, 2003; revised May 25, 2004. This work was presented at the Power Electronics Specialist Conference (PESC), Acapulco, Mexico, June 15–19, 2003. This work was supported by the National Science Foundation under Grant 01 202 531. Recommended by Associate Editor J. Ojo.

P. Beccue and S. Pekarek were with the Department of Electrical Engineering, University of Missouri-Rolla (UMR), Rolla, MO 65409 USA. They are now with the Department of Electrical Engineering, Purdue University, West Lafayette, IN, 47907 USA (e-mail: spekarek@purdue.edu).

D. Stutts is with the Department of Mechanical Engineering, University of Missouri-Rolla (UMR), Rolla, MO 65409 USA.

J. Neely was with the Department of Electrical Engineering, University of Missouri-Rolla (UMR), Rolla, MO 65409 USA. He is now with the Intelligent Systems and Robotics Center, Sandia National Laboratories, Albuquerque, NM 87185 USA.

Digital Object Identifier 10.1109/TPEL.2004.839810

$\boldsymbol{i}_{qh} \in \mathbb{R}^{g-1}$	Stator current harmonics coefficients in matrix form (not including the fundamental even Fourier series component).
v_{sensor}	Output voltage of sensor amplifier voltage.
x_{eqy}	Component of sensor voltage attributed to yth harmonic of torsional vibration (even Fourier series harmonic).
x_{edy}	Component of sensor voltage attributed to yth harmonic of torsional vibration (odd Fourier series harmonic).
G	Cost function.
$\boldsymbol{Q}, \boldsymbol{R}$	Matrices containing weighting factors for cost-function analysis.
Z^*	Set of nonnegative integers.

I. Introduction

OVER THE past several years, significant effort has been placed on developing control techniques to mitigate torque ripple created by permanent magnet synchronous machines (PMSM) [1]–[9]. In most approaches, a drive system is used to provide optimized current excitation based upon measured harmonics of back-emf, and in some instances, harmonics of cogging torque. In [2], a method is set forth to select current harmonics to cancel low frequency torque harmonics. In [3], a method of selecting current harmonics is derived to cancel torque harmonics while simultaneously minimizing the rms stator current. In [4], this same idea is extended with an additional design constraint of a fixed inverter voltage. In [2]–[4], the harmonics attributed to cogging torque are neglected. In [5], the harmonics due to cogging torque are considered and a procedure is derived to establish current excitation subject to a user-defined arbitrary weighting between the constraints of minimizing rms current and minimizing torque ripple harmonics.

In general, the methods presented in [2]–[5] require exact knowledge of the machine back-emf and cogging torque harmonics. There is no feedback in the control loop, which leads to sensitivity of the control to imperfect knowledge and variation in machine parameters. There has been an effort to develop control methods that include the use of torque estimators and observers as part of the control [6]–[8]. However, in these techniques, extensive knowledge of the machine is required, and the system remains susceptible to parameter variation. In [9], a feedback-based vibration/noise mitigation control scheme is proposed for a surface-mount PMSM with sinusoidal back emf. Therein, an accelerometer or microphone is used to provide vibration/noise feedback from the machine/mount. The feedback signal is used to adjust the commanded quadrature-axis stator current to mitigate detected vibration/noise.

In this paper, closed-loop controllers that mitigate the stator torsional vibrations resulting from torque ripple produced by a surface mount PMSM with nonsinusoidal back-emf are described. The controllers manipulate stator current harmonics in response to measured frame torsional vibration. Stator current harmonic amplitudes/phases are determined using algorithms based upon cost-function minimization. To measure torque ripple-induced frame torsional vibration, a sensor has been designed using a polymer-based piezoelectric film. The sensor is easy to construct and incorporate into a drive system, has a wide bandwidth, and is relatively inexpensive. Simulation and experimental results are provided to demonstrate the effectiveness of the proposed measurement and control techniques.

II. Sources of Torsional Vibration

The acoustic noise/vibration of the machine studied in this research is dominated by stator torsional rotation that results from harmonics of electromagnetic torque. The machine is sold commercially for use as a propulsion motor for hybrid-electric motorcycles and solar-powered vehicles. The back-emf contains multiple harmonics and cogging torque is significant. Control of vibration/noise levels is obtained through control of stator current harmonics. The machine is designed using three full-pitch concentrated stator phase windings (one slot/pole/phase) that are wye-connected. The voltage equations of the windings are expressed as

$$v_{as} = r_s i_{as} + p\lambda_{as} \tag{1}$$

$$v_{bs} = r_s i_{bs} + p\lambda_{bs} \tag{2}$$

$$v_{cs} = r_s i_{cs} + p\lambda_{cs} \tag{3}$$

where v_{xs} represents a phase to neutral voltage, r_s a phase resistance, i_{xs} a phase current, λ_{xs} a phase flux linkage, and p denotes differentiation with respect to time.

The phase flux linkages in (1)–(3) are a function of the magnetic flux produced by the phase currents as well as the flux produced by permanent magnets in the rotor. Herein the flux linkages are expressed as

$$\lambda_{as} = L_{asas} i_{as} + L_{asbs} i_{bs} + L_{ascs} i_{cs} + \lambda_{asm} \tag{4}$$

$$\lambda_{bs} = L_{bsas} i_{as} + L_{bsbs} i_{bs} + L_{bscs} i_{cs} + \lambda_{bsm} \tag{5}$$

$$\lambda_{cs} = L_{csas} i_{as} + L_{csbs} i_{bs} + L_{cscs} i_{cs} + \lambda_{csm} \tag{6}$$

where L_{xsys} are the "x" to "y" phase mutual inductances and the terms $\lambda_{asm}, \lambda_{bsm}, \lambda_{csm}$ represent the influence of the flux of the permanent magnets on the respective stator windings. These are represented in terms of a Fourier series as

$$\lambda_{asm} = \lambda_{\text{mag}} \sum_{m \in M} \kappa_{em} \sin(m\theta_r) \tag{7}$$

$$\lambda_{bsm} = \lambda_{\text{mag}} \sum_{m \in M} \kappa_{em} \sin(m(\theta_r - 120^\circ)) \tag{8}$$

$$\lambda_{csm} = \lambda_{\text{mag}} \sum_{m \in M} \kappa_{em} \sin(m(\theta_r + 120^\circ)) \tag{9}$$

where κ_{em} is the magnitude of the mth Fourier harmonic coefficient and λ_{mag} is a coefficient defined such that $\kappa_{e1} = 1$. The set $M = \{m = 2x + 1 : x \in Z*, \kappa_{\text{em}} \neq 0\}$, where $Z*$ is the set of nonnegative integers and the angle θ_r represents the electrical rotor position that is defined such that at $\theta_r = 0$, no fundamental rotor flux links the as-winding. The subscript "e" denotes a relationship to the machine back-emf.

A closed-form expression for the electromagnetic torque is established using an energy balance approach [10], which yields

$$T_e = \frac{P\lambda_{\text{mag}}}{2}\left[i_{as}\left(\sum_{m\in M} m\kappa_{\text{em}}\cos(m\theta_r)\right) + i_{bs}\left(\sum_{m\in M} m\kappa_{\text{em}}\cos(m(\theta_r-120^\circ))\right) + i_{cs}\left(\sum_{m\in M} m\kappa_{\text{em}}\cos(m(\theta_r+120^\circ))\right)\right] + T_{\text{cog}} \tag{10}$$

where P is the number of poles and T_{cog} represents the torque resulting from interaction of the permanent magnets and the stator teeth (cogging torque). Since the machine is designed using an integer number of slots/pole/phase, the cogging torque is a function of the sixth order harmonics of rotor angular position. Mathematically, the cogging torque can be expressed as

$$T_{\text{cog}} = \sum_{y\in Y} T_{cqy}\cos(y\theta_r) + T_{cdy}\sin(y\theta_r) \tag{11}$$

where $Y = \{y = 6x : x \in Z*, \mathbf{T}_{cqd} \neq 0\}$. For subsequent analysis, it is assumed that the stator currents can be represented in series form as

$$i_{as} = \sum_{n\in N} \kappa_{iqn}\cos(n\theta_r) + \kappa_{idn}\sin(n\theta_r) \tag{12}$$

$$i_{bs} = \sum_{n\in N} \kappa_{iqn}\cos(n(\theta_r-120^\circ)) + \kappa_{idn}\sin(n(\theta_r-120^\circ)) \tag{13}$$

$$i_{cs} = \sum_{n\in N} \kappa_{iqn}\cos(n(\theta_r+120^\circ)) + \kappa_{idn}\sin(n(\theta_r+120^\circ)). \tag{14}$$

The set $N=\{n=2x+1, n\neq 3z : x\in Z*, z\in Z*, \kappa_{iqn}\neq 0\}$.

Substituting (12)–(14) into (10) and manipulating the final result, the electromagnetic torque may be represented as

$$T_e = \bar{\boldsymbol{T}}_e + \sum_{y\in Y} T_{eqy}\cos(y\theta_r) + T_{edy}\sin(y\theta_r) \tag{15}$$

where

$$\bar{\boldsymbol{T}}_e = \frac{3P\lambda_{\text{mag}}}{4}\sum_{n\in N}\kappa_{en}\kappa_{iqn} \tag{16}$$

represents the average electromagnetic torque produced by the machine, and

$$T_{eqy} = \frac{3P\lambda_{\text{mag}}}{4}\sum_{n\in N}(\kappa_{e|y-n|} + \kappa_{e|y+n|})\kappa_{iqn} + T_{cqy} \tag{17}$$

$$T_{edy} = \frac{3P\lambda_{\text{mag}}}{4}\sum_{n\in N}(\kappa_{e|y-n|} + \kappa_{e|y+n|})\kappa_{idn} + T_{cdy} \tag{18}$$

represent coefficients of Fourier series of the torque ripple series expressed in trigonometric form. Prior to proceeding, it is important to clarify the components that are provided in (17) and (18). Specifically, some analysts use the term "torque ripple" to describe harmonics resulting from stator current and rotor back-emf harmonic interaction [first term on the right-hand side of the equal sign in (17) and (18)]. Herein, we use the term torque ripple to describe the sum of the harmonics resulting from the stator current/rotor back-emf harmonic interaction and cogging torque harmonics.

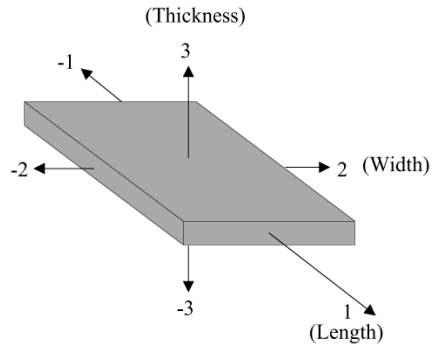

Fig. 1. Illustration of piezoelectric polymer film.

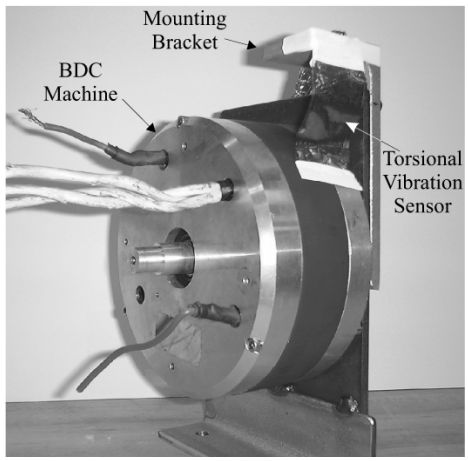

Fig. 2. Torque ripple sensor mounting configuration.

III. Measuring Torsional Vibration

To provide feedback for a control loop, a polyvinylidene fluoride (PVDF) film was selected to measure the effect of stator torsional vibration. The PVDF film is a piezoelectric polymer. An illustration of the film is shown in Fig. 1. In this application, a voltage is produced in the direction in which the material is poled (in this case the three-axis) in response to the strain transverse to the poled direction (one- or two-axis). The relationship between strain and voltage is linear, with a proportionality constant related to the material composition and the thickness of the film. The dynamic range over which the material translates stress into a voltage is between 0.001 Hz and 10^9 Hz [11]. To measure torsional vibration, a 7.6 $\times$ 3.8 $\times$ 0.0025 cm strip of PVDF is placed between the motor and a fixed point on the mount using an adhesive tape, as shown in Fig. 2. The PVDF is coated with silver ink and leads are soldered to each side to detect the induced voltage. In practice, mounting the strip must be done with care. Specifically, to achieve repeatable values of sensor voltage (which is important when designing an amplifier or in instances where torque ripple produced by multiple machines are to be compared) the sensor must be placed in an

TABLE I
MACHINE PARAMETERS

$L_{ms} = 17.56uH$	$L_{ls} = 1.96uH$	$r_s = 0.022\,\Omega$	$\lambda_m = 0.0112\,Vs$
$P = 12$	$\kappa_{e1} = 1.0$	$\kappa_{e3} = -7.18 \cdot 10^{-2}$	$\kappa_{e5} = 1.05 \cdot 10^{-2}$
$\kappa_{e7} = -9.02 \cdot 10^{-4}$	$\kappa_{e11} = 5.95 \cdot 10^{-4}$	$\kappa_{e13} = 1.81 \cdot 10^{-4}$	$T_{cq6} = 1.23$ Nm
$T_{cd6} = 0.0$ Nm	$T_{cq12} = 0.22$ Nm	$T_{cd12} = 0.0$ Nm	Rated Speed = 3600 RPM
Rated Power = 5 kW	Outer Diameter = 17.8 cm	Length = 8.8 cm	Slots/Pole/Phase = 1

identical location each time. In the laboratory, this has been achieved using pen markings on the mount and motor. For commercial use, where tape adhesives and pen markings may not be practical, one can attach the sensor to a flexible plate (soft steel, plastic) that bends with stator vibration. The plate can be attached to the mount and motor housing using set screws for permanent placement.

As mounted in Fig. 2, the voltage produced by the sensor was measured to confirm that the signal resulting from stator torsional vibration is proportional to torque ripple. For validation, the rotor speed was held constant and rotor position was selected so that $T_{cd6} = 0$. The stator current harmonics were controlled such that $\kappa_{idn} = 0$. Further, κ_{iq1} was fixed at 16.5 A and κ_{iq5} was varied from 0 to 11 A. From (17), under the test conditions specified, the magnitude of the sixth harmonic torque can be expressed as

$$T_{eq6} = \frac{3P\lambda_{\text{image}}}{4}[(\kappa_{e5} + \kappa_{e7})16.5 + (\kappa_{e1} + \kappa_{e11})\kappa_{iq5}] + T_{cq6}. \tag{19}$$

Based upon the parameters of the machine shown in Table I, where the values of cogging torque amplitude have been determined from measurement, the expected values of torque ripple amplitude for the test obtained from simulation are shown in Table II. Also shown are the amplitudes of the voltage obtained from the sensor. For clarity, the data in Table II is plotted in Fig. 3. To generate the plot, the voltage and torque ripple amplitudes at $\kappa_{iq5} = 0$ A have been subtracted from subsequent values and the results normalized to the $\kappa_{iq5} = 11$ A value.

From Fig. 3, it can be seen that a linear increase in the amplitude of the sixth harmonic of torque ripple produces a linear increase in the sensor voltage, which confirms that the sensor is an effective torsional vibration/voltage transducer. It is important to note that the output of the sensor is a voltage (not Nm). The sensor measures stator torsional vibrations that result from torque ripple. These measurements are dependent upon the response of the stator frame/mechanical system to torque ripple, which can be frequency dependent. Therefore, without precise knowledge of the mechanical response to torque ripple at each frequency, one cannot obtain an accurate voltage/Nm conversion. Although this limits the use of the sensor to measure exact values of torque ripple amplitude, it does not diminish its usefulness as a sensor for feedback-based vibration mitigation.

The voltages shown in Table II reflect measured values obtained using a sensor constructed in the UM-Rolla laboratory. This sensor has been used for all studies contained in this paper. In over two years of tests on multiple mount systems it has faired well. Thus, a conclusion has been that it is robust. Important constraints for sensor design include a thermal limit of 90 °C and a mechanical limit (pressure) of 50 MPa for the PVDF film. Subsequent to performing studies documented in this paper, it has been found that PVDF strips (with electrodes attached) are manufactured commercially and are used in various applications, including traffic sensors and counter switches [12]. A 17 × 2.2 × 0.005 cm commercial strip has been tested using the arrangement in Fig. 2. The voltages produced have been roughly an order of magnitude greater than the in-house sensor under the same operating conditions. Tests to gauge the level of sensitivity of the commercial strip have been performed. For the tests, measured values of the back-emf and cogging torque amplitudes were used to determine values of the stator current harmonics to adjust torque ripple harmonic values using (19). Stator currents were commanded to adjust the level of torque ripple to roughly 10 mNm, which was validated using an in-line torque transducer. The output of the commercial sensor was roughly 20 mV. The minimum level of torque ripple was limited to 10 mNm due to limits of accuracy that the current can be controlled. The signal/noise ratio of the piezoelectric sensor was computed at this operating point to be greater than 20 dB. Thus, through testing ripple of roughly 10 mNm.

TABLE II
MEASURED AND CALCULATED TORQUE RIPPLE VALUES

κ_{iq5} (A)		0.0	2.2	4.4	6.6	8.8	11.0
T_{e6}	Calculated (Nm)	1.25	1.47	1.69	1.91	2.13	2.36
	Measured (mV)	50.9	52.3	53.9	55.5	57.2	58.7

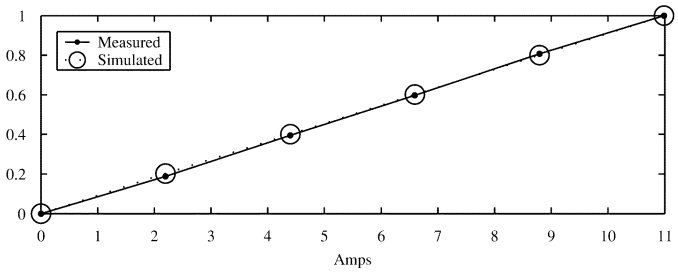

Fig. 3. Comparison of measured and simulated sixth harmonic torque ripple amplitude versus i_{q5}.

IV. SENSOR CONDITIONING

As configured, the torsional vibration sensor has a source voltage-series capacitance equivalent circuit that is shown in

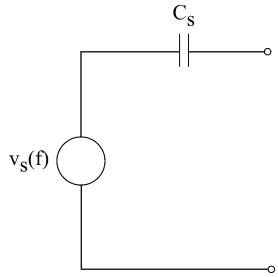

Fig. 4. Electrical equivalent of PVDF film.

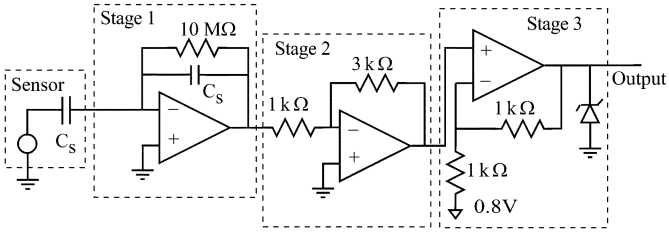

Fig. 5. Amplifier from sensor to processor input.

Fig. 4 [11]. To be utilized in a control loop, the induced voltage must be detected, amplified, and conditioned. One design issue is to convert the relatively low voltage produced across the film (tens of mV) to a signal that can be used for digital control. A second design issue is to overcome the capacitive source impedance, which, without the use of external circuit components, limits the ability to capture low frequency signals. A circuit used to perform amplification and signal conditioning is shown in Fig. 5. Therein, a three-stage op-amp circuit is shown between the sensor and the analog input to a processor board. The first stage of the amplifier is designed to effectively cancel the series capacitance of the sensor, the second is used to provide gain, and third is to add offset and to limit the voltage so that the input to the processor is between 0 and 3.3 V.

The output of the amplifier circuit shown in Fig. 5 is a time-domain signal that contains all of the torsional harmonics. For closed-loop control, knowledge of individual harmonic amplitudes related to (T_{eqy} and T_{edy}) is required. In order to extract these values, the output voltage of the amplifier is multiplied (within the processor) with sine and cosine functions of the desired torsional harmonic components. The product is then input into a "leaky" integrator in order to extract the respective amplitudes. Specifically

$$x_{eqy} = \int \left[v_{\text{sensor}} \cos(y\theta_r) - \varepsilon x_{eqy}\right] dt \tag{20}$$

$$x_{edy} = \int \left[v_{\text{sensor}} \sin(y\theta_r) - \varepsilon x_{edy}\right] dt \tag{21}$$

are voltages that are representative of torsional vibration harmonics attributed to T_{eqy} and T_{edy}.

V. Mitigating Torsional Vibration

As shown in Section III, the stator torsional vibration of the machine studied is linearly related to torque ripple. Therefore, mitigation of the vibration is achieved through mitigation of torque ripple. Most existing methods to mitigate torque ripple in nonsinusoidal back-emf machines use analytical closed-form expressions to determine current harmonics that force T_{eqy} and T_{edy} to zero. In this application, current harmonics are determined using a controller that is based upon cost function minimization. Depending upon the requirements of the drive, there are alternatives to implementing cost function-based control. As a basis for the methods considered herein, it is assumed that a set of f torque harmonics are to be controlled using $g \geq f+1$ current harmonics and that average torque is a command to the drive system.

A. Precise Control of Average Torque

To derive the first control technique, it is assumed that precise control of average torque is required. As will be shown, this translates into a requirement that there is precise knowledge of the back-emf coefficients. In practice, both conditions are rare, so the result is somewhat academic. Nonetheless, the control method derived provides a possible solution for custom applications and sets the stage for considering alternative methods.

To derive the controller, (17) and (18) are represented in matrix form as

$$\boldsymbol{T}_{\text{eq}} = \boldsymbol{K}_{e1}\boldsymbol{i}_q + \boldsymbol{T}_{cq} \tag{22}$$

$$\boldsymbol{T}_{ed} = \boldsymbol{K}_{e1}\boldsymbol{i}_d + \boldsymbol{T}_{cd} \tag{23}$$

where $\boldsymbol{T}_{\text{eq}} \in \mathbb{R}^f$ and $\boldsymbol{T}_{ed} \in \mathbb{R}^f$ contain torque harmonic coefficients (including cogging torque), $\boldsymbol{K}_{e1} \in \mathbb{R}^{f\times g}$ is a matrix that contains coefficients of back-emf [scaled by (0.75P λ_{mag})], $\boldsymbol{i}_q \in \mathbb{R}^g$ and $\boldsymbol{i}_d \in \mathbb{R}^g$ are vectors that contain coefficients of stator current harmonics, and $\boldsymbol{T}_{cq} \in \mathbb{R}^f$ and $\boldsymbol{T}_{cd} \in \mathbb{R}^f$ are vectors that contain the coefficients of cogging torque. Commanded average torque is expressed in terms of stator current harmonic amplitudes as

$$\boldsymbol{K}_{e2}^t \boldsymbol{i}_q = \bar{\boldsymbol{T}}_e^* \tag{24}$$

where $\boldsymbol{K}_{e2} \in \mathbb{R}^g$ is obtained from (16).

A scalar cost function is defined in terms of the torque ripple harmonic amplitudes as

$$G = \boldsymbol{T}_{\text{eq}}^t Q T_{\text{eq}} + \boldsymbol{T}_{ed}^t Q T_{ed} \tag{25}$$

where $\boldsymbol{Q} \in \mathbb{R}^{f\times f}$ is a diagonal matrix that contains components to weight overall cost in favor of one harmonic over another. Minimization of G is accomplished by manipulating stator currents. To represent G in terms of current harmonic amplitudes, (22) and (23) are used to expand (25) into a form

$$\begin{aligned} G = {} & (\boldsymbol{K}_{e1}\boldsymbol{i}_q + \boldsymbol{T}_{cq})^t \boldsymbol{Q}(\boldsymbol{K}_{e1}\boldsymbol{i}_q + \boldsymbol{T}_{cq}) \\ & + (\boldsymbol{K}_{e1}\boldsymbol{i}_d + \boldsymbol{T}_{cd})^t \boldsymbol{Q}(\boldsymbol{K}_{e1}\boldsymbol{i}_d + \boldsymbol{T}_{cd}). \end{aligned} \tag{26}$$

A solution for $\boldsymbol{i}_q$ and $\boldsymbol{i}_d$ that minimizes (26) subject to achieving commanded average torque (24) is derived using a projected gradient algorithm [13]. Herein, the algorithm is expressed as a state-model

$$\frac{d}{dt}\boldsymbol{i}_q = -\alpha P \nabla_{iq} G, \quad \boldsymbol{K}_{e2}^t \boldsymbol{i}_q(0) = \bar{\boldsymbol{T}}_e^* \tag{27}$$

$$\frac{d}{dt}\boldsymbol{i}_d = -\alpha \nabla_{id} G \tag{28}$$

where $\nabla_{iq}G$ and $\nabla_{id}G$ represent the gradient of G with respect to $\boldsymbol{i}_q$ and $\boldsymbol{i}_d$, respectively, and

$$P = \boldsymbol{i}_n - \boldsymbol{K}_{e2}^t \left(\boldsymbol{K}_{e2}\boldsymbol{K}_{e2}^t\right)^{-1} \boldsymbol{K}_{e2} \tag{29}$$

is a matrix that projects the gradient of G along the solution to (24) so that the commanded average torque is maintained. A projection is not required in (28), since the constraint does not involve $\boldsymbol{i}_d$. The scalar α is a control parameter used to adjust the time constant of the controller [13].

In application, $\nabla_{iq}G$ and $\nabla_{id}G$ are determined from the torsional vibration sensor. Specifically, from (26), $\nabla_{iq}G$ and $\nabla_{id}G$ are first expressed as

$$\nabla_{iq}G = 2\boldsymbol{K}_{e1}^t\mathbf{Q}(\boldsymbol{K}_{e1}\boldsymbol{i}_q + \boldsymbol{T}_{cq}) \tag{30}$$

$$\nabla_{id}G = 2\boldsymbol{K}_{e1}^t\boldsymbol{Q}(\boldsymbol{K}_{e1}\boldsymbol{i}_d + \boldsymbol{T}_{cd}). \tag{31}$$

Using (22) and (23), (30) and (31) are simplified to

$$\nabla_{iq}G = 2\boldsymbol{K}_{e1}^t QT_{\mathrm{eq}} \tag{32}$$

$$\nabla_{id}G = 2\boldsymbol{K}_{e1}^t QT_{ed}. \tag{33}$$

The values $\boldsymbol{x}_q$ and $\boldsymbol{x}_d$ obtained from (20) and (21) are used to represent the torque ripple coefficients in (32) and (33), wherein the final algorithm is of the form

$$\frac{d}{dt}\boldsymbol{i}_q = -\alpha 2PK_{e1}^t Qx_q, \quad \boldsymbol{K}_{e2}^t\boldsymbol{i}_q(0) = \bar{\boldsymbol{T}}_e^* \tag{34}$$

$$\frac{d}{dt}\boldsymbol{i}_d = -\alpha 2\boldsymbol{K}_{e1}^t Qx_d. \tag{35}$$

Provided $\boldsymbol{i}_q(0)$ is a solution to (24), $\boldsymbol{i}_q$ will remain a solution to the constraint for all time [13]. It is noted that precise knowledge of back-emf harmonics is not required to mitigate torsional vibration due to torque ripple. In fact, from (34) and (35) it is seen that the algorithm ceases only when $\boldsymbol{x}_q$ and $\boldsymbol{x}_d$ become zero vectors. However, precise knowledge of back-emf is required to achieve an exact value of commanded average torque. A block diagram depicting the projected gradient-based control that is used to determine $\boldsymbol{i}_q$ is shown in Fig. 6. A similar diagram can be drawn to depict the control used to determine $\boldsymbol{i}_d$.

The controller shown in Fig. 6 was implemented in the simulation of the PMSM described in Table I. The controller was implemented such that the average torque is maintained and the sixth torque ripple harmonic is eliminated through the manipulation of the fundamental and the fifth harmonic of current. The torque ripple and phase current were recorded before and after the torque ripple feedback control was implemented. Prior to mitigation, the fundamental was adjusted to achieve commanded average torque. The simulation was performed with the machine operating at 333 rpm. The motor drive was modeled using an inverter operating under hysteresis current control. Results of the simulation before and after the mitigation control are shown in Figs. 7 and 8.

Viewing simulated responses after the ripple mitigation control is executed, it is seen that a significant fifth harmonic is present in the stator current waveform and the sixth harmonic of torque ripple is eliminated, while the average torque is maintained. For further insight, a frequency domain plot of the torque spectrum was obtained for the simulation and is shown in Fig. 9.

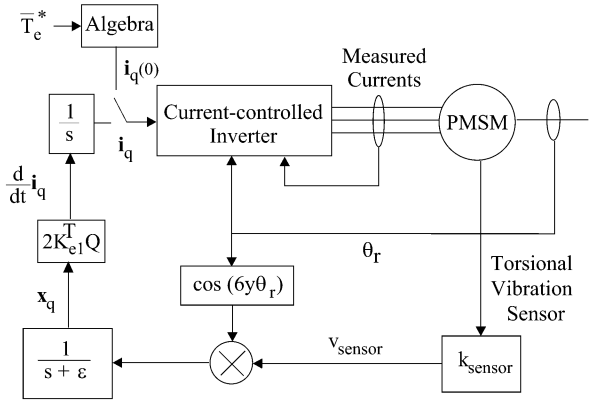

Fig. 6. Diagram of torque ripple controller for q-axis based upon projected gradient algorithm (constrained optimization).vs

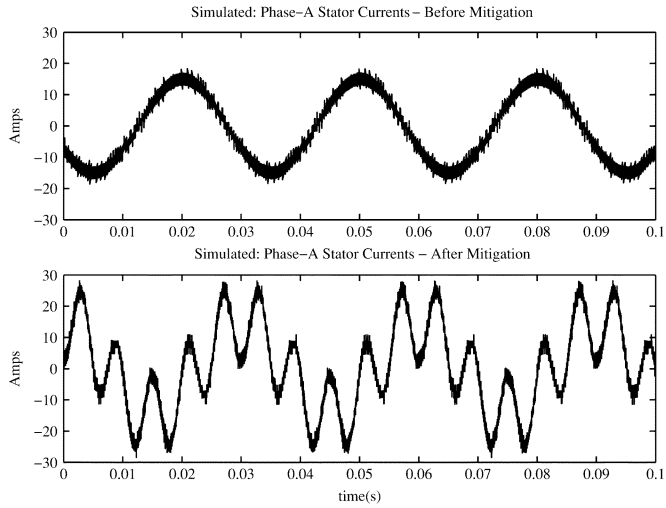

Fig. 7. Simulated stator currents before and after implementation of the torque ripple mitigation controller.

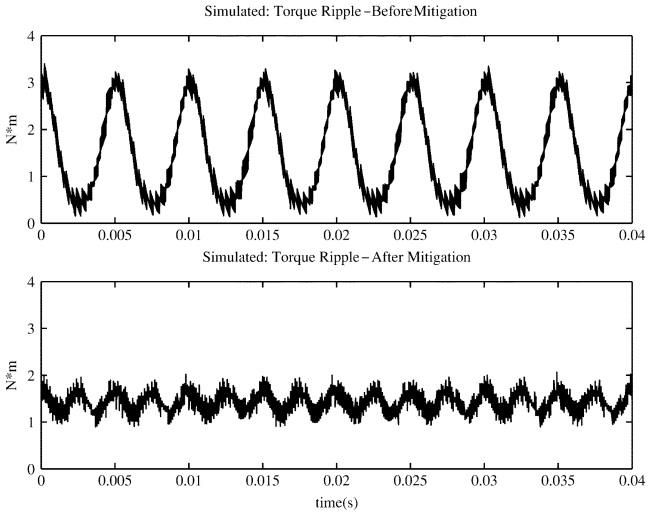

Fig. 8. Simulated torque ripple before and after implementation of the torque ripple mitigation controller.

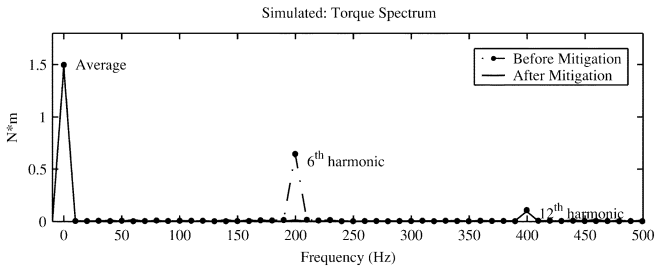

Fig. 9. Simulated torque ripple amplitude versus frequency before and after implementation of torque ripple mitigation controller.

B. Approximate Control of Average Torque

In most commercial applications, knowledge of back-emf coefficients is imprecise (due to saturation, variability across a design platform, temperature dependence, etc.). In such applications, an alternative control can be derived by eliminating the constraint on $\mathbf{i}_q$ (since exact values of average torque cannot be met without precise knowledge of back-emf). To perform unconstrained optimization, the fundamental component of stator current, κ_{iq1}, is not selected algorithmically. Rather, it is used to track the desired average torque. The harmonic components of current are used to mitigate torque ripple. To derive the controller, (22) is first rewritten as

$$\boldsymbol{T}_{\rm eq} = \kappa_{iq1}\boldsymbol{K}_{e3} + \boldsymbol{K}_{e4}\boldsymbol{i}_{qh} + \boldsymbol{T}_{cq} \tag{36}$$

where $\boldsymbol{K}_{e3} \in \mathbb{R}^f$ and $\boldsymbol{K}_{e4} \in \mathbb{R}^{f\times(g-1)}$ contain scaled back-emf coefficients and $\boldsymbol{i}_{qh} \in \mathbb{R}^{g-1}$ is a vector representing the current harmonics (not including the fundamental). The expression (36) is then substituted into (25), and the gradient of G is taken with respect to the current vector $\boldsymbol{i}_{qh}$. This sequence of operations yields

$$\nabla_{iqh}G = 2\boldsymbol{K}_{e4}^t\boldsymbol{Q}(\kappa_{iq1}\boldsymbol{K}_{e3} + \boldsymbol{K}_{e4}\boldsymbol{i}_{qh} + \boldsymbol{T}_{cq}). \tag{37}$$

From (36), (37) may be expressed as

$$\nabla_{iq}G = 2\boldsymbol{K}_{e4}^t Q T_{\rm eq}. \tag{38}$$

A solution for $\boldsymbol{i}_{qh}$ that mitigates torque ripple is found using a gradient algorithm [13]. Herein, the algorithm is expressed as a state-model

$$\frac{d}{dt}\boldsymbol{i}_{qh} = -\alpha 2\boldsymbol{K}_{e4}^t Q T_{\rm eq}. \tag{39}$$

The values $\boldsymbol{x}_q$ from (20) are used to represent the torque ripple coefficients in (39), wherein the algorithm used is of the form

$$\frac{d}{dt}\boldsymbol{i}_{qh} = -\alpha 2\boldsymbol{K}_{e4}^t Q x_q. \tag{40}$$

The algorithm to determine $\boldsymbol{i}_d$ is identical to that shown in (35), since constraints are not placed on d-axis currents in either case.

A block-diagram of the unconstrained control used to determine $\boldsymbol{i}_{qh}$ is shown in Fig. 10.

C. Minimum Current-Minimum Torsional Vibration

In [5], Lagrange multipliers are used to establish current excitation subject to a user-defined arbitrary weighting between the constraints of minimizing rms current and minimizing torque

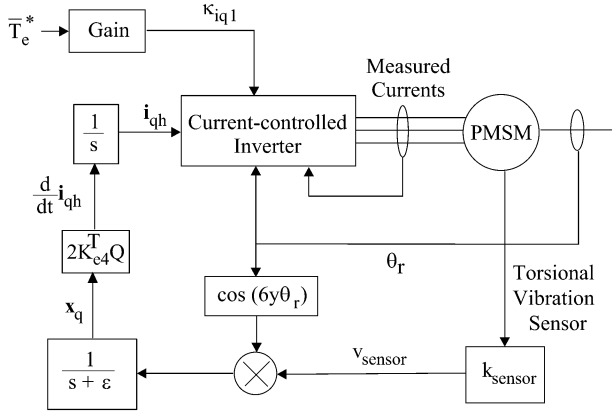

Fig. 10. Diagram of torque ripple controller for q-axis based upon gradient algorithm (unconstrained optimization).

ripple harmonics. To derive a minimum-rms-current minimum-torsional vibration (MCMR) controller that uses feedback, a cost-function approach can be used wherein (25) is replaced with

$$G = \boldsymbol{T}_{\rm eq}^t Q T_{\rm eq} + \boldsymbol{T}_{ed}^t Q T_{\rm eq} + \beta\left(\boldsymbol{i}_q^t R i_q + \boldsymbol{i}_d^t R i_d\right). \tag{41}$$

In (41) $R \in \mathbb{R}^{g\times g}$ is a diagonal weighting matrix and β is chosen to weight the cost in terms of minimum current rms versus minimum torque ripple. Gradient algorithms can be used to determine controllers that minimize (41). The resulting algorithms are similar in form to (34)–(35) or (40).

VI. Hardware Implementation

Of the techniques presented, the control derived assuming imprecise knowledge of back-emf coefficients is of most practical interest. Therefore, the unconstrained control was implemented in hardware using the machine shown in Fig. 2. For the given application the stator torsional vibration was measured using the mechanical setup shown in Fig. 2. The dimensions of the sensor used were 7.6 × 3.8 × 0.0025 cm. The output voltage of the sensor amplifier circuit (Fig. 4) was input to the A/D ports on the DSP (sampling rate of A/D is 2 kHz). The hardware testing was performed using an inverter operating under hysteresis current control with the machine operating at 333 rpm. For commercial applications, the machine is controlled with a drive consisting of metal-oxide-semiconductor field effect transistor (MOSFET) switches. However for the tests described herein, the machine was operated using insulated gate bipolar transistors (IGBTs). Due to their relatively low switching frequency, 0.4 mH inductors were placed in series with the stator phase windings to facilitate current based switching regulation. For stator current feedback within hysteresis control, the current was measured using a F.W. Bell CLN-50 current sensor. The machine speed was maintained by coupling the motor to a Magtrol HD-715-8 hysteresis-brake dynamometer operated in a speed control mode. Magnaloy 100 series couplings were used to couple the motor and dynamometer.

For the implementation, a TMS 320LF2407 DSP was used as the controller. The algorithm was programmed using fixed-point arithmetic in a C language format. Without implementing the code in assembly language, the speed of execution of the DSP

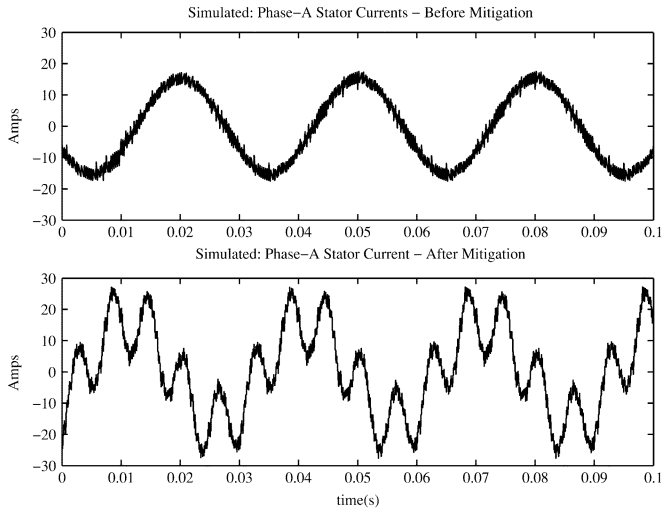

Fig. 11. Simulated stator currents before and after implementation of the torque ripple mitigation controller.

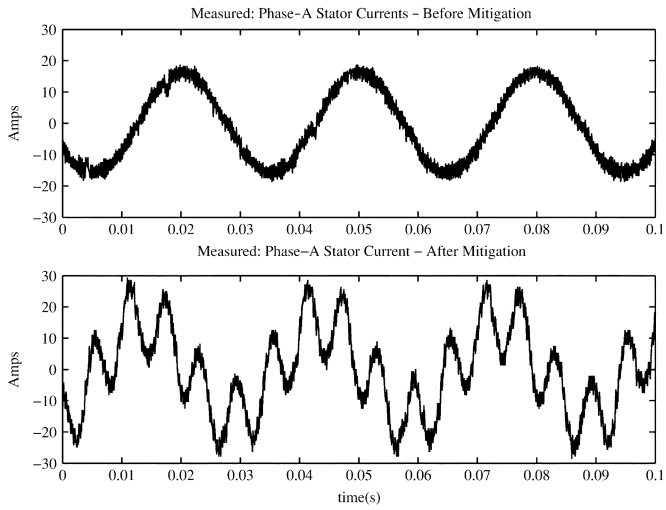

Fig. 12. Measured stator currents before and after implementation of the torque ripple mitigation controller.

limited testing to monitoring one torsional harmonic and manipulating three current harmonics. Specifically, the controller was such that κ_{iq1} was used to track average torque (1.5 Nm), while mitigation of the sixth torque ripple induced harmonic was accomplished using

$$\frac{d}{dt}\kappa_{iq5} = -\alpha 2(\kappa_{e1} + \kappa_{e11}) q_{11} x_{eq6} \tag{42}$$

$$\frac{d}{dt}\begin{bmatrix} \kappa_{id1} \\ \kappa_{id5} \end{bmatrix} = -\alpha 2 \begin{bmatrix} \kappa_{e5} + \kappa_{e7} \\ \kappa_{e1} + \kappa_{e11} \end{bmatrix} q_{11} x_{ed6}. \tag{43}$$

The torque ripple and phase current measurements were recorded before and after the torque ripple feedback control was implemented. Prior to mitigation, κ_{iq1} was adjusted to achieve the commanded average torque. The remaining harmonic coefficients were initially set to zero. Results of a time-domain simulation of the drive are provided for comparison. Within the drive system model, the control algorithm was simulated using fixed-point arithmetic and the sampling interrupts that are present within the DSP implementation.

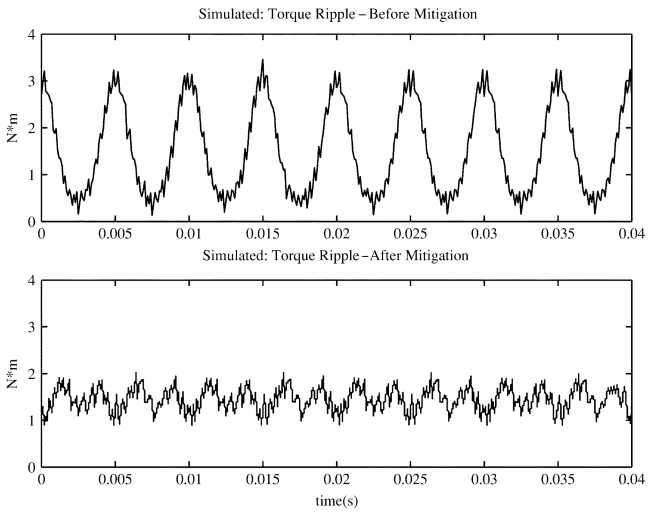

Fig. 13. Simulated torque ripple before and after implementation of the torque ripple mitigation controller.

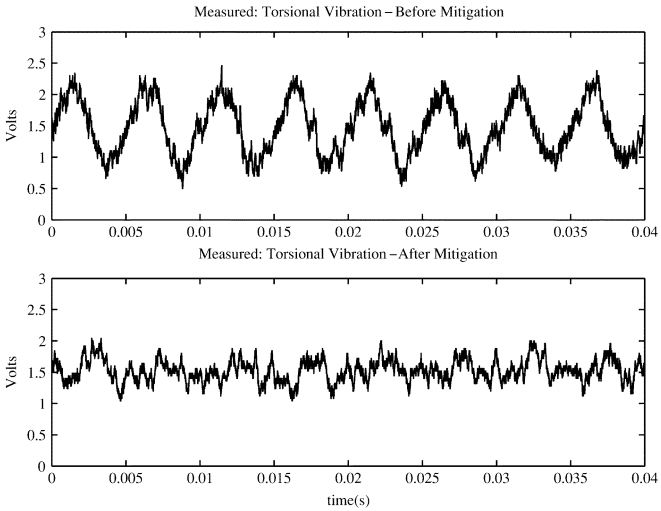

Fig. 14. Measured torsional vibration before and after implementation of the torque ripple mitigation controller (2 kHz DSP processing).

Results of the current and torsional harmonics before and after the mitigation control are shown in Figs. 11–14. The currents shown in Fig. 12 were obtained using a Tektronix A6303 current probe/Tektronix AM 503A current probe amplifier. The sensor voltage shown in Fig. 14 was measured at the output of the amplifier circuit using an HP 1160A 10:1 voltage probe, and captured using an HP infinium 54 815A oscilloscope. For this motor, the tested load condition of 1.5 Nm at 333 RPM reflects a relatively light load level. This motor is rated for 5 kW at 3600 RPM. The speed and torque level were chosen for two reasons. First, the execution rate of the DSP for the given algorithm is roughly 2 kHz. Therefore, an operating point was chosen where the sixth harmonic of electromagnetic torque was roughly 1 decade below (200 Hz) in order to avoid controller/DSP sampling interactions. The selection of the 1.5 Nm was chosen due to the limits of inverter hardware. Specifically, the ratings of the inverters in the UM-Rolla power electronics laboratory are 30 A. From Figs. 11 and 12, one can see that when torque mitigation control is implemented, the fifth harmonic current is significant and leads to peak currents close to 30 A.

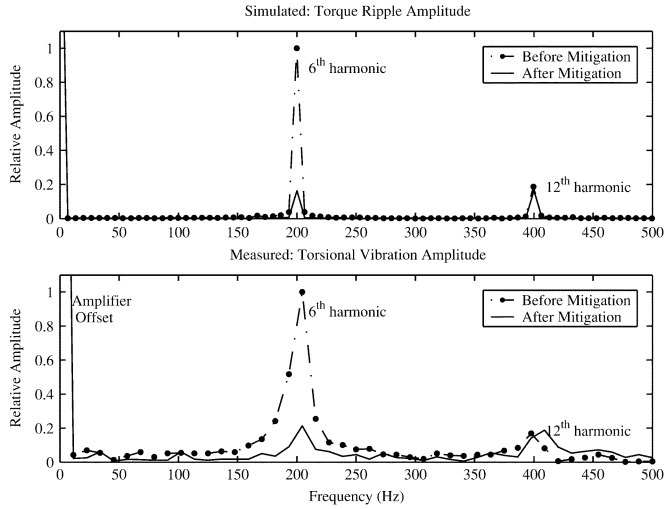

Fig. 15. Simulated torque ripple and measured torsional vibration amplitude versus frequency before and after implementation of torque ripple mitigation controller (2 kHz DSP processing).

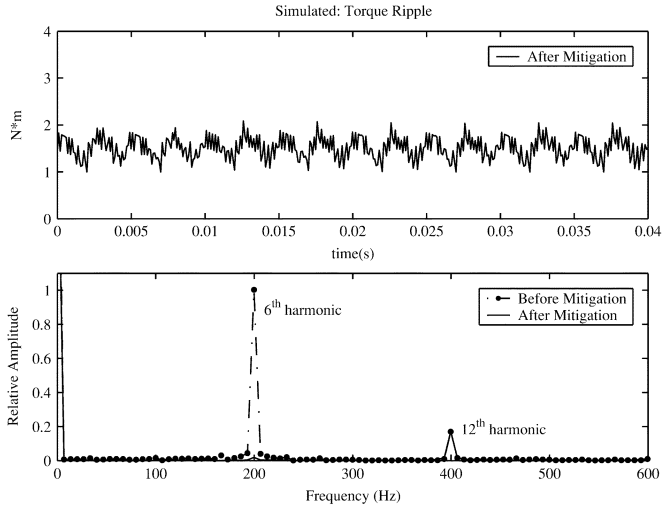

Fig. 16. Simulated torque ripple after mitigation and torque ripple amplitude before and after mitigation (50 kHz DSP processing).

For the 1.5-Nm/333-rpm operating point, the machine is operated in a region where saturation is minimal. Magnetic saturation would introduce operating-point dependent back-emf coefficients. To mimic the effects saturation would have on the proposed approach, a randomness was introduced into the back emf coefficients defined in the controller ($\boldsymbol{K}_{e4}^{t}$ and $\boldsymbol{K}_{e1}^{t}$). Specifically, within the controller each of the back emf coefficients (which in this case were known and are shown in Table I) was multiplied by a different random number between 0.1 and 0.5. Thus, although the machine was not operated in a region of saturation, the effect saturation would have on the control was represented. It is important to note that saturation can have an effect on cogging torque amplitude. However, a convenience of the given approach is that knowledge of the cogging torque amplitude is not required for the control algorithm proposed.

Viewing measured (torsional vibration) and simulated (torque ripple) responses after the ripple mitigation control was executed, it is seen that a significant fifth harmonic is present in the stator current waveform and the sixth harmonic of torque ripple (torsional vibration) was greatly reduced. For further insight into the controller effectiveness, a frequency domain plot was obtained for both the simulation and hardware tests and is shown in Fig. 15.

The frequency domain plot shows nearly an 80% reduction in magnitude of sixth torque ripple harmonic (simulation) and torsional vibration (measured) after the control was applied in both the simulation and hardware. It is also noted that although the 12th harmonic of torque was not controlled, the measured and simulated values are nearly identical for all tests performed.

Theoretically, complete mitigation of the sixth torque harmonic is expected. However, in practice, the ability of the control to completely mitigate the sixth harmonic was limited by the sampling speed of the DSP and the accuracy of using fixed-point arithmetic. For the experiments performed, the sampling speed of the DSP was roughly 2 kHz. To demonstrate increased effectiveness of the control, a simulation study was performed wherein the DSP sampling frequency is increased from 2 to 50 kHz and all control algorithm calculations are performed using floating-point operations. The torque ripple and the frequency domain plot resulting from the simulation are shown in Fig. 16. From the figure, it can be seen that the sixth harmonic torque ripple is eliminated completely.

Although mitigation of the sixth harmonic is achieved, one can see from Fig. 16 that torque ripple remains. The two major components that are evident in the simulation are the 12th torque ripple harmonic and a high frequency torque ripple due to the switching of the inverter (i.e., switching harmonics of the stator currents interacting with the back-emf to produce torque ripple). In fact, the 12th harmonic value (.35 Nm) can be unacceptably high for some applications. Though we have not been able to validate in hardware using the existing DSP, simulations have been performed that show mitigation of both the sixth and 12th harmonic can be achieved using the fifth and 11th harmonics of stator currents. Therefore, we believe all low-frequency components are controllable given sufficient processing power. In many applications, the switching frequency-based torque ripple harmonics are of less interest, since for existing semiconductor technologies they are out of the audible range (i.e., $>$20 kHz). However, in some applications, such as naval ship propulsion, high frequency torque ripple can be of interest. The mitigation of high frequency torque ripple resulting from switching is a topic of ongoing investigation. An important point is that the proposed sensor can measure high frequency vibrations, which provides a place to start the investigation.

VII. Conclusion

New controllers have been derived to mitigate torsional vibration due to torque ripple in a surface mount PMSM with nonsinusoidal back-emf. To provide feedback, a frame torsional vibration sensor has also been designed. The sensor and controllers are relatively straightforward to implement, and can be applied to surface mount PMSMs with arbitrary magnet and stator winding configurations. Hardware and simulation results demonstrate the effectiveness of the proposed methods.

REFERENCES

[1] T. M. Jahns and W. L. Soong, "Pulsating torque minimization techniques for permanent magnet ac motor drives—A review," *IEEE Trans. Ind. Electron.*, vol. 43, no. 2, pp. 321–329, Apr. 1996.

[2] H. Le-Huy, R. Perret, and R. Feuillet, "Minimization of torque ripple in brushless dc motor drives," *IEEE Trans. Ind. Appl.*, vol. IA-22, no. 4, pp. 803–813, Jul./Aug. 1986.

[3] C. Kang and I. Ha, "An efficient torque control algorithm for BLDCM with a general shape back-emf," in *Proc. Power Electronics Specialists Conf.*, 1993, pp. 451–457.

[4] D. C. Hanselman, "Minimum torque ripple, maximum efficiency excitation of brushless permanent magnet motors," *IEEE Trans. Ind. Electron.*, vol. 41, no. 3, pp. 292–300, Jun. 1994.

[5] P. L. Chapman, S. D. Sudhoff, and C. A. Whitcomb, "Optimal current control strategies for surface-mounted permanent-magnet synchronous machine drives," *IEEE Trans. Energy Conv.*, vol. 14, no. 4, pp. 1043–1050, Dec. 1999.

[6] F. Colamartino, C. Marchand, and A. Razek, "Considerations of non-sinusoidal field distribution in a permanent magnet synchronous motor control," in *Proc. Inst. Elect. Eng. Conf. Power Electronics Variable-Speed Drives*, Oct. 1994, pp. 508–513.

[7] T. S. Low, K. J. Tseng, T. H. Lee, K. W. Lim, and K. S. Lock, "Strategy for the instantaneous torque control of permanent-magnet brushless dc drives," in *Proc. Inst. Elect. Eng. B*, vol. 137, Nov. 1990, pp. 355–363.

[8] N. Matsui, T. Makino, and H. Satoh, "Auto-compensation of torque ripple of dc motor by torque observer," in *Proc. IEEE Industry Applications Soc. Annu. Meeting*, Dearborn, MI, Sep. 1991, pp. 305–311.

[9] T. Su, S. Hattori, M. Ishida, and T. Hori, "Suppression control method for torque vibration of AC motor utilizing repetitive controller with fourier transform," *IEEE Trans. Ind. Appl.*, vol. 38, no. 5, pp. 1316–1325, Sept./Oct. 2002.

[10] P. C. Krause, O. Wasynczuk, and S. D. Sudhoff, *Analysis of Electric Machinery*. Piscataway, NJ: IEEE Press, 1995.

[11] *Technical Manual*, 1999.

[12] Piezo Film Sensors Technical Manual, MSI Piezo Products. (1999). [Online]. Available: http://www.msiusa.com/piezo/products.asp

[13] S. Zak and E. Chong, *An Introduction to Optimization*. New York: Wiley, 1996.

Philip B. Beccue (S'00) received the B.S. and M.S. degrees in electrical engineering from the University of Missouri-Rolla, in 2001 and 2002, respectively, and is currently pursuing the Ph.D. degree in electrical engineering at Purdue University, West Lafayette, IN.

His research interest is currently focused on permanent magnet synchronous motor control.

Mr. Beccue received the NSF IGERT Fellowship.

Jason Neely received the B.S. and M.S. degrees in electrical engineering from the University of Missouri-Rolla, in 1999 and 2001, respectively, with emphasis in electromagnetic compatibility, controls, and electric drives.

He is currently with the Intelligent Systems and Robotics Center, Sandia National Laboratory, Albuquerque, NM.

Mr. Neely received the NSF IGERT Fellowship.

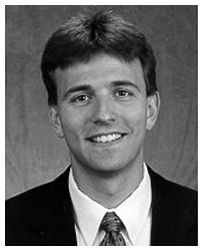

Steve Pekarek (S'89–M'96) received the Ph.D. degree in electrical engineering from Purdue University, West Lafayette, IN, in 1996.

From 1997–2004, he was an Assistant/Associate Professor of electrical and computer engineering with the University of Missouri-Rolla. He is now an Associate Professor of electrical and computer engineering at Purdue University. As a faculty member he has been the Principal Investigator on a number of successful research programs including projects for the Navy, Air Force, Ford Motor Co., and Delphi Automotive Systems. The primary focus of these investigations has been the analysis and design of electric machinery and power electronic based architectures for finite inertia power and propulsion systems.

Dr. Pekarek is a Member of the Electric Machinery Committee of the IEEE Power Engineering Society, the IEEE Power Electronics Society, and the Society of Automotive Engineers.

Dan Stutts was born in Canton, GA, on January 9, 1959. He received the B.S. and M.S. degrees in mechanical engineering from Louisiana State University, Baton Rouge, LA, in 1983 and 1987 respectively, and the Ph.D. degree in mechanical engineering from Purdue University, West Lafayette, IN, in 1990.

In 1991, he joined the Faculty of Mechanical Engineering and Engineering Mechanics, University of Missouri-Rolla, and was promoted to Associate Professor in 1997. He has worked in the area of piezoelectric actuator design and modeling since 1993.